



Enhanced field induced martensitic phase transition and magnetocaloric effect in $\text{Ni}_{55}\text{Mn}_{20}\text{Ga}_{25}$ metallic foams

Carlo Paolo Sasso^{a,*}, Peiqi Zheng^b, Vittorio Basso^a, Peter Müllner^c, David C. Dunand^b

^a Istituto Nazionale di Ricerca Metrologica (INRIM), Electromagnetics Division, Strada delle Cacce 91, I-10135 Torino, Italy

^b Department of Materials Science and Engineering, Northwestern University, Evanston, IL 60208, USA

^c Department of Materials Science and Engineering, Boise State University, Boise, ID 83725, USA

ARTICLE INFO

Article history:

Received 4 January 2011

Received in revised form

14 February 2011

Accepted 21 February 2011

Available online 21 March 2011

Keywords:

A. Magnetic intermetallics

B. Magnetic properties

B. Martensitic transformations

F. Calorimetry

ABSTRACT

The high surface/volume ratio and mechanical stability under cyclic strain makes polycrystalline Ni–Mn–Ga metallic foams attractive for magnetic refrigeration. By means of comparison with a polycrystalline bulk material, we have demonstrated that the porous structure of $\text{Ni}_{54.8}\text{Mn}_{20.2}\text{Ga}_{25.0}$ open-cells metallic foams (porosity varying between 44% and 58%) reduces the temperature span of the phase transition and increases the magnetocaloric effect (MCE). MCE was investigated using calorimetry in a magnetic field. Temperature scan and isothermal experiments have shown a 0.8 K T^{-1} shift of the phase transition temperature and a maximum irreversible entropy change of $2.5 \text{ J kg}^{-1} \text{ K}^{-1}$. The results indicate that metallic foams can represent a good approach for enhancing field induced phase transitions in magnetic refrigeration applications.

© 2011 Elsevier Ltd. All rights reserved.

1. Introduction

Recently, an enhanced magnetocaloric effect was observed among magnetic materials presenting a first-order magnetic phase transition. In this case, the latent heat of the phase transition contributes to the magnetocaloric effect (MCE) [1]. Examples are: $\text{Gd}_2(\text{Si,Ge})_4$ [2]; $\text{La}(\text{Fe,Si})_{13}$ [3]; MnAs [4]; $(\text{Mn,Fe})_2(\text{P,Ge})$ [5] and alloys of the Heusler family including $\text{Ni}_2\text{Mn}(\text{Ga,Sb,In,Sn})$ [6]. In these materials, a magnetic field shifts the equilibrium of the two phases, inducing the growth of the magnetic phase at the expenses of the non-magnetic phase.

Some of the prototypes for magnetic cooling devices are based on the Active Magnetic Regenerative Refrigeration (AMRR) cycle [7] in which the magnetic regenerating material exchanges heat with a fluid which is alternatively flowing to the hot and to the cold thermal baths. In order to improve the thermal contact between the fluid and the regenerating material, one has to increase the surface to volume ratio. This is generally done by shaping the materials in the form of thin foils or small spheres [8]. Furthermore, in a refrigerating device the material is cycled between the two phases and subjected to several phase transitions that are normally accompanied by large changes of the lattice parameters including

isotropic volume changes of the unit cell (e.g. $\text{La}(\text{FeSi})_{13}$ exhibits a 1% volume expansion) or very large anisotropic lattice strains and symmetry changes of the unit cell (Ni_2MnGa undergoes a cubic to tetragonal phase transition with Bain strains of the order of 6% [9]). Under thermal cycling these strains introduce cracks which can fracture the active material even after a few cycles between the two structural phases [10].

In this work, we investigate magnetocaloric properties and details of the phase transition of a Ni–Mn–Ga metallic foam prepared by replication casting [11] which may offer a solution to the two issues mentioned above. The open porosity allows a fluid to percolate through, making them attractive for magnetic refrigeration because of their high surface to volume ratio. An additional benefit is that foaming reduces the constraints imposed by grain boundaries, thus enhancing the magneto-strain performances of polycrystal samples [11] without any cracking or serious reduction in the magnetoelastic performances, even after thousands of magnetic-field-induced deformation cycles.

Ni_2MnGa martensitic alloy is a multifunctional material where a magnetic field can induce large strains, connected to a structural phase growth or martensitic variant reorientation [12,13], as well as a magnetocaloric effect [14,15]. According to the phase diagram of the $\text{Ni}_{50+x}\text{Mn}_{25-x}\text{Ga}_{25}$ off-stoichiometric composition where Mn is partially substituted by an excess of Ni, the curie temperature and the martensitic phase transition coincide in the small range where x varies between 4.5 and 5 at % [16]. For this range of compositions,

* Corresponding author. Tel.: +39 0113919821; fax: +39 0113919834.
E-mail address: c.sasso@inrim.it (C.P. Sasso).

the structural phase transition occurs between a low-temperature ferromagnetic-martensite phase and a high-temperature paramagnetic-austenite phase.

In the present paper we investigate $\text{Ni}_{54.8}\text{Mn}_{20.2}\text{Ga}_{25.0}$ metallic foams with a 45–54% open porosity which allows for percolation of a fluid through the material. The composition was chosen in the range where structural and magnetic phase transition coincide and the magnetocaloric effect is potentially large [15]. The MCE is compared with that of a bulk polycrystal with the same composition. Magnetocaloric properties are investigated by a differential calorimeter operating under a magnetic field and able to measure either specific heat, $c_p(T, H)$, under constant magnetic field, H , or isothermal entropy change, $\Delta s(H, T)$, induced by changing the magnetic field [17]. The magnetocaloric characterization shows that the different porosities investigated here have a small effect on the MCE but, with respect to bulk polycrystal, foams show a substantial enhancement of the MCE and a completely different evolution of the phase transition. This confirms and extends the general improvement in magnetic-field-induced strain achieved in foams by removing the constraints due to the grain boundaries.

2. Experimental

Three polycrystalline Ni–Mn–Ga foam samples (A–B–C) with open porosities of 44, 48 and 58%, respectively, were produced by replication casting, using spherical sodium aluminate powders (350–500 μm), as previously described [11]. The average composition of all the three samples is $\text{Ni}_{54.80 \pm 0.21}\text{Mn}_{20.15 \pm 0.03}\text{Ga}_{25.06 \pm 0.23}$ and was determined simultaneously using a Hitachi S3400 N-II scanning electron microscope (SEM) equipped with an integrated Oxford EDS system, keeping instrument parameters (accelerating voltage, probe current, working distance) constant. A control bulk sample with identical composition was cast from the same batch of pure materials (99%Ni, 99%Mn, 99%Ga). The samples were cut into $5 \times 5 \times 1 \text{ mm}^3$ specimens fitting into the calorimeter sensor. At this composition, the Curie temperature is expected to coincide with the martensite-to-austenite phase transition temperature so that the material transforms between ferromagnetic-martensite and paramagnetic-austenite phases [16,15]. The characterization of the magnetocaloric effect can be performed by determining the specific entropy $s(H, T)$ as a function of temperature and magnetic field. The entropy is given by integration of specific heat under different constant magnetic field, $c_p(H, T) = Tds/dT$. The differential calorimeter used here operates in a magnetic field under either temperature scanning or isothermal conditions and therefore allows to measure both the specific heat under a constant magnetic field and the isothermal entropy change induced by a magnetic field. Miniaturized thermoelectric Peltier cells are employed as heat flux sensors (RMT 1MD04-031-12, size $5 \times 5 \times 2.3 \text{ mm}^3$), with a resolution of about $1 \mu\text{W}$. The calorimeter operates in the temperature range 240–365 K. After a calibration procedure, the calorimeter gives the heat flux exchanged between the sample and the thermal bath, q_s , at the temperature T_b . As presented in reference [17], by studying the problem of heat diffusion in the calorimeter, we have found expressions for: i) q_s corrected for the intrinsic kinetics of the sensing cells due to their heat capacity (introducing a characteristic time constant); ii) the temperature T_s of the sample which systematically lags or anticipates T_b . The setup is placed in the gap of an electromagnet and characterization was carried out at a maximum field of $\mu_0 H = 1.2 \text{ T}$. The magnetic field was oriented parallel to the largest face of the sample. The temperature of the thermal bath is digitally controlled and therefore it is possible to perform measurements at well defined scanning rate (up to almost 15 K/min) or under isothermal condition at a very low level of thermal fluctuations (within 10 mK). For all the

samples, q_s was determined either at a temperature scan rate of 0.1 K s^{-1} (6 K/min) or under ‘constant temperature’-‘varying magnetic field’, with $\frac{dH}{dt} \approx 13 \text{ mT s}^{-1}$. From temperature scanning experiments, the specific heat $c_p(T, H)$ was determined from $q_s(T, H)$:

$$c_p(T, H) = \frac{1}{m} \frac{q_s(T, H)}{\dot{T}_s} \quad (1)$$

Specific entropy curves, $s(T, H)$ were obtained by integrating $c_p(T, H)/T$. When the phase transition is not affected by hysteresis, the isothermal entropy change, $\Delta s_H(T)$, and the adiabatic temperature change, $\Delta T_s(H)$, due to the magnetic field, can be estimated from the entropy curves performed at constant magnetic field. When hysteresis is present in the phase transition, this is partially true because $\Delta s_H(T)$ and $\Delta T_s(H)$ will depend not only on the temperature of measurement but also from its previous history. For these reasons, we have compared the $\Delta s_H(T)$, as can be computed by subtracting the entropy curves for each T value, with isothermal measurements of the entropy change induced by magnetic field as can be obtained from $q_s(H, T)$ by the formula:

$$\Delta s_H(T) = \frac{1}{m} \int_{t_0}^{t_1} \frac{q_s(T, H)}{T_s} dt, \quad (2)$$

where the integration limits (t_0 and t_1) are set in order to sum up all the heat flux connected to the application and, eventually, removal of the magnetic field. In the next section, we will show, by analyzing the isothermal measurements, that the largest isothermal entropy change predicted by the isothermal difference of entropy curves can be achieved only following a specific sequence of temperature variation and magnetic field exposure.

3. Results and discussion

The curves of $c_p(T)$ at zero magnetic field (Fig. 1) show that the martensitic phase transition is widely distributed over a temperature range of approximately 60 K. The spread of the phase transition is in contrast to the single crystals studied in [15] and is likely due to the disorder introduced by the polycrystalline structure of the samples, which hinders the phase transition evolution. Nevertheless, the metallic foams have a narrower phase transition, with

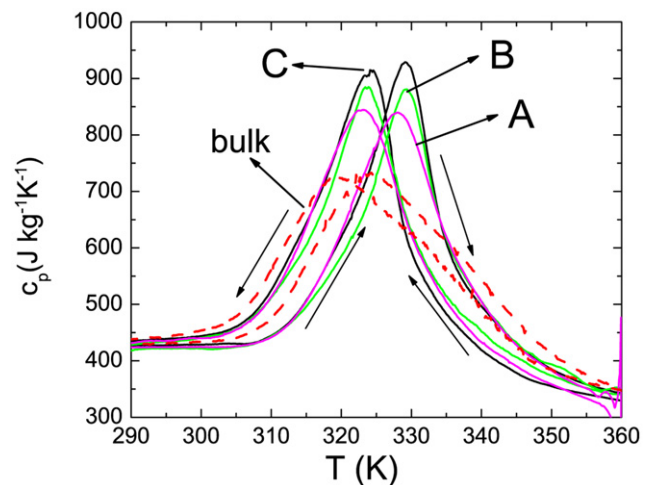


Fig. 1. Comparison between the specific heat without magnetic field of foamed samples A–B–C (solid lines) and bulk (dashed line). The arrows identify the heating and cooling curves.

respect to the polycrystalline bulk material, and higher c_p peaks which increase with the porosity level. This picture corresponds to the fact that the phase transition is less hindered in the metallic foams because there are less grain boundaries pinning the phase interfaces.

The specific heat of martensite and austenite just below and above the phase transition are $c_p^M \approx 420 \text{ Jkg}^{-1}\text{K}^{-1}$ and $c_p^A \approx 350 \text{ Jkg}^{-1}\text{K}^{-1}$, respectively. By integrating the c_p curves (Fig. 1), the specific entropy curves ($s(T) - s_0$) were obtained where s_0 is the entropy at the beginning of the integration. In Fig. 2, the specific entropies of the sample C and that of the bulk sample are compared.

The entropy of the bulk sample has a smaller slope, as can be predicted from the shape of its c_p vs. T curve, nevertheless, the total specific entropy change due to the martensitic phase transition is conserved. In order to evaluate the entropy change between the two phases, we have assumed a constant value for the specific heat of martensite and austenite in the 100 K temperature interval analyzed. With this assumption the specific entropy of each phase is a logarithmic function,

$$s_i(T) = c_p^i \ln\left(\frac{T}{T_0}\right) + \Delta s_0^i, \quad (3)$$

where $T_0 = 270 \text{ K}$ is the temperature at which we start to integrate the specific heat curves, $i = M$ or A for martensite or austenite, respectively, and $\Delta s_0^i = (s_0^i(T_0) - s_0^M(T_0))$ is equal to zero for $i = M$ and to the difference between the entropy of the two phases at T_0 for $i = A$. Introducing into Eq. (3) the values of specific heat mentioned above, as depicted in Fig. 2, it is possible to evaluate an entropy change of $27.1 \text{ Jkg}^{-1} \text{ K}^{-1}$ at 330 K , in the middle of the martensite-to-austenite phase transition. This value compares to

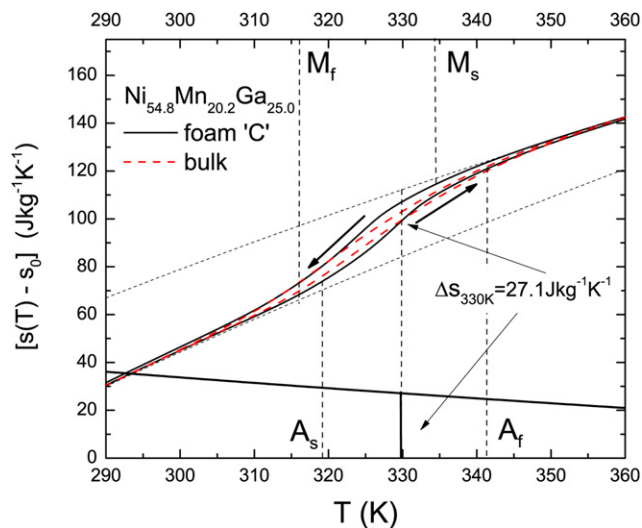


Fig. 2. Specific entropy for the samples **C** and **bulk** obtained integrating the specific heat of Fig. 1. Dashed lines are the logarithmic analytical curves of the specific entropy for the single phases, austenite (A) and martensite (M), achieved by assuming a constant specific heat for the single phases: $s_i(T) = c_p^i \ln\left(\frac{T}{T_0}\right) + \Delta s_0^i$, where $T_0 = 270 \text{ K}$ is the temperature at which we start integrating the specific heat, $i = M$ or A and $\Delta s_0^i = (s_0^i(T_0) - s_0^M(T_0))$ is the difference between the entropy of the two phases and the entropy of martensite at T_0 . The values used for the parameters are: $c_p^A = 350 \text{ Jkg}^{-1}\text{K}^{-1}$; $\Delta s_0^A = 0 \text{ Jkg}^{-1}\text{K}^{-1}$; $c_p^M = 410 \text{ Jkg}^{-1}\text{K}^{-1}$; $\Delta s_0^M = 48 \text{ Jkg}^{-1}\text{K}^{-1}$. The thicker solid line at the bottom of the figure is the difference between the logarithmic curves and represents the total entropy change between the two phases vs. temperature. At 330 K , in the middle of the M-A phase transition, the entropy change is about $27.1 \text{ Jkg}^{-1} \text{ K}^{-1}$. In the figure also the start and finish martensitic phase transition temperatures have been roughly estimated by taking them as the temperatures at which 10% and 90% of the phase is transformed: $A_s \approx 319.2 \text{ K}$; $A_f \approx 340.2 \text{ K}$; $M_s \approx 334.3 \text{ K}$; $M_f \approx 311.6 \text{ K}$.

the entropy change of single crystal with a similar composition [15] and other Heusler alloys [18–20]. Specific entropy curves were also used to estimate the characteristic temperatures of the phase transition, as reported in the caption of Fig. 2. In Fig. 3, the specific entropy of the foamed sample C under a magnetic field $\mu_0 H = 1.2 \text{ T}$ and without magnetic field are compared.

The specific entropy was obtained by integrating the specific heat over T shown in the inset of Fig. 3. The application of the magnetic field shifts the $c_p(T, H)$ and $s(T, H)$ curves to higher temperatures, demonstrating that magnetic field stabilizes the ferromagnetic-martensite phase. This shift is 0.8 K T^{-1} , equaling that reported by other authors for single crystals with similar compositions [14]. For all the porous samples, we have achieved similar results. In principle, by subtracting the curve obtained without magnetic field, $s(T, 0)$, from that achieved under magnetic field H , $s(T, H)$, we can compute the isothermal entropy change induced by the magnetic field H , $\Delta s_H(T) = s(T, H) - s(T, 0)$. We have reported isothermal entropy change computed with this method (solid lines) for the sample “C” in Fig. 4. The negative values of the curves imply a direct magnetocaloric effect where the magnetic field reduces the entropy. Under a 1.2 T maximum magnetic field, the peaks (heating and cooling) of $\Delta s_H(T)$ have a full width at half maximum of about 15 K . The other porous samples give very similar results, with small differences in the maximum entropy change.

In order to interpret these curves, in Fig. 4, we have also reported isothermal entropy change measurements performed with our calorimeter (Eq. (2)) for a change of the magnetic field from 0 T to 1.2 T . As already discussed in [21], the total isothermal entropy change that can be achieved in a material presenting an hysteretic first order magneto-structural phase transition depends strongly on the sequence of the applied temperature and magnetic field changes. In particular, the entropy change is larger when temperature and magnetic field act concordantly on the phase transition. In our case, martensite is the ferromagnetic phase and is stabilized or furthered by the application of a magnetic field. Therefore we expect that, during cooling from austenite, the application of the magnetic field is more effective on the growth of the martensite phase and therefore the entropy change is larger, whereas, during heating from the martensite phase, the same effect is achieved by removing a previously applied magnetic field. The isothermal

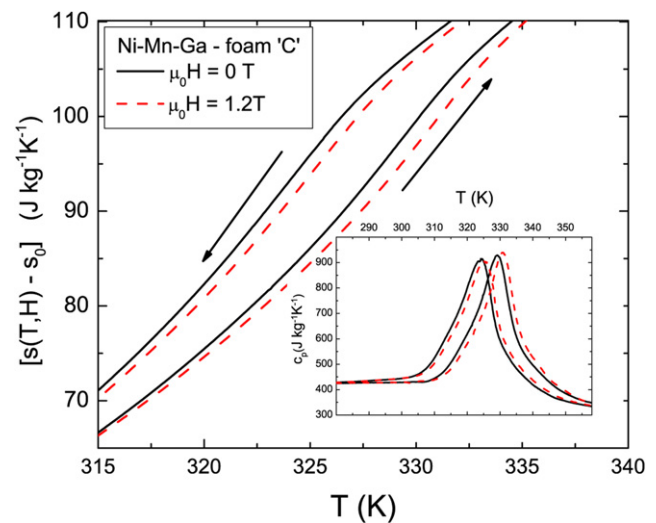


Fig. 3. Specific entropy of sample C around the phase transition measured with (dashed line) and without the magnetic field (solid line). Inset - Specific heat of sample C measured with (dashed line) and without the magnetic field (solid line).

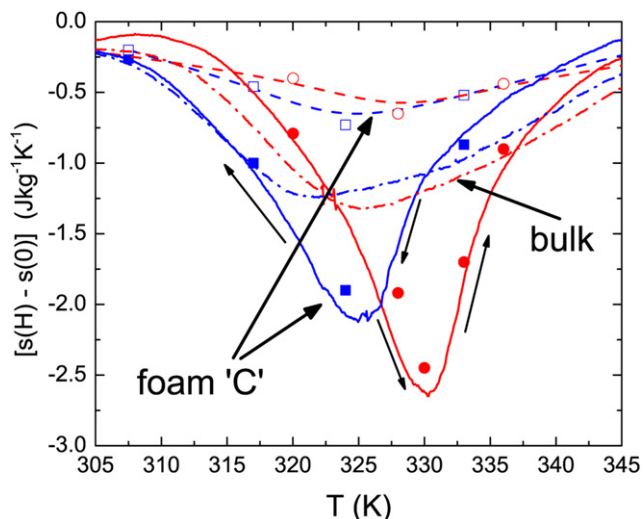


Fig. 4. Solid lines - $\Delta s_H(T)$ computed from the entropy curves of Fig. 3 for the sample C by subtraction $\Delta s_H(T) = s(T, H) - s(T, 0)$. Dash-dot lines - $-\Delta s_H(T)$ for bulk sample obtained from entropy subtraction. Full symbols - Isothermal measurements of $\Delta s_H(T)$ for the foamed sample C obtained by: red-dots - using the *hr* protocol; blue-square - using the *ca* protocol. Open symbols - reversible isothermal entropy change of the foamed sample C obtained cycling the magnetic field after the *hr* protocol (circles) and the *cr* protocol (square). Dashed lines - Guide for the eyes connecting open symbols.

measurements have been performed following two distinct measurement protocols: *protocol ca* (cooling-applying field) where austenite phase is obtained by heating to a sufficiently high-temperature and then the temperature is decreased down to the measurement temperature, T_0 , then the magnetic field is applied at a rate of 13 mT/s; *protocol hr* (heating-removing field) where temperature is decreased to a value sufficient to have only martensite in the sample, the full magnetic field is applied and then the temperature is increased to the measuring temperature, T_0 , then the magnetic field is removed at a rate of 13 mT/s. After each protocol, the magnetic field has been cycled in order to measure the reversible entropy change. The first change of the magnetic field produces a larger entropy change which follow the solid curves (for foam C, Fig. 4) obtained by the temperature scan method. On the other hand, the reversible entropy change is lower because of the hysteresis in the phase transition. Nevertheless, the small hysteresis in the reversible behavior (two peaks are visible in the dashed lines used simply as guides for the eyes in Fig. 4) is showing that the magnetic field is likely still inducing a reversible change in the phase fraction at each cycle and the reversible entropy change is not only due to the contribute of the conventional magnetocaloric effect. In Fig. 4, we have also compared the entropy change for the bulk sample with that of the sample C, taken as representative of the three porous samples. It is noteworthy that the entropy change for the foam is doubled with respect to that of the bulk sample. This result is a direct consequence of porosity on the evolution of the phase transition, as evidenced by the comparison between the bulk and foamed samples in Figs. 1 and 2. In particular, the bulk sample shows a smaller peak of the $c_p(T)$ (Fig. 1) and a more slanted hysteresis loop of the specific entropy (Fig. 2). Both these behaviors denote a more hindered phase transition in the bulk than in the porous material. Together with the fact that the isothermal entropy change is connected to the field induced phase shift of the phase transition temperatures (see Fig. 3 and the method for evaluating entropy change from that curves) and that the magnitude of this shift is equal in bulk and porous samples, we deduce that a smaller slope of the entropy curve will lead to a lower entropy change. Therefore, the larger entropy change in porous samples is connected to the

facilitated phase transition. The martensite phase transition involves strain and volume mismatches at the boundaries between different structural phases that must be accommodated. Analogously to the effect of pores size on the incompatibilities between twinned grains, which enhances the magnetic-field-induced strain in magnetic shape memory alloys [11,22], the presence of pores enhances the phase transition evolution, which lead to a larger MCE.

4. Conclusions

We have analyzed, by means of calorimetry in a magnetic field, the phase transition evolution and the magnetocaloric effect of metallic foams with composition $\text{Ni}_{54.8}\text{Mn}_{20.2}\text{Ga}_{25.0}$. The magnetic-field-induced positive shift of 0.8 K T^{-1} of the phase transition is in agreement with values of bulk alloys with similar compositions. Comparing polycrystalline bulk material and the metallic foams demonstrates that the porosity has a general beneficial impact on the phase transition evolution. In particular, a two fold increase of the field induced entropy change (magnetocaloric effect) was observed, as well as a narrowing of the phase transition (Fig. 2). This fact is in agreement with previous observations that the field induced strain in Ni–Mn–Ga foams of different composition is strongly enhanced by porosity. The presence of pores between material grains enables the deformation of polycrystals under the field induced motion of twin boundaries and a magnetic-field-induced strain comparable to single crystals was observed [11]. In the case of the structural phase transition, the strains and volume changes at lattice level is better accommodated in the presence of pores which reduce the incompatibility between neighboring grains. The different degrees of porosity investigated (between 44% and 58%) have not introduced significant differences in the magnetocaloric effect. The general interpretation, where hysteresis introduces a dependence of the field induced entropy change from the history of the applied temperature and magnetic field, has been confirmed and therefore the available entropy change, as can be computed from temperature scan measurements, is obtained only following the right experimental protocol where temperature and magnetic field act concordantly on the phase transition (heating-removing magnetic field or cooling-applying magnetic field). In addition to the benefits on the magnetocaloric applications introduced by materials in the form of open-cell foams such as their resistance under cyclic deformations and their large surface/volume ratio, this work shows that introduction of porosity is a promising method for reducing mismatch stresses in magnetostructural phase transitions, usually introducing large deformations of the grains, and therefore increasing the magnetocaloric response.

Acknowledgment

PZ, PM, and DCD acknowledge financial support of the National Science Foundation, Division of Materials Research grant No. NSF-DMR 0804984 (Boise State University) and grant No. DMR-0805064 (Northwestern University).

CPS and VB acknowledge that the research leading to these results received funding from the European Community 7th Framework Programme under grant agreement 214864 (project SSEEC).

References

- [1] Pecharsky VK, Gschneidner KA, Pecharsky AO, Tishin AM. Thermodynamics of the magnetocaloric effect. *Phys Rev B* 2001;64(14):144406. doi:10.1103/PhysRevB.64.144406.
- [2] Pecharsky VK, Gschneidner Jr KA. Giant magnetocaloric effect in $\text{Gd}_5(\text{Si}_2\text{Ge}_2)$. *Phys Rev Lett* 1997;78(23):4494–7. doi:10.1103/PhysRevLett.78.4494.

- [3] Fujita A, Fujieda S, Hasegawa Y, Fukamichi K. Itinerant-electron metamagnetic transition and large magnetocaloric effects in $\text{La}(\text{Fe}_x\text{Si}_{1-x})_{13}$ compounds and their hydrides. *Phys Rev B* 2003;67(10):104416. doi:10.1103/PhysRevB.67.104416.
- [4] Wada H, Tanabe Y. Giant magnetocaloric effect of $\text{MnAs}_{1-x}\text{Si}_x$. *Appl Phys Lett* 2001;79(20):3302–4. doi:10.1063/1.1419048.
- [5] Liu DM, Huang QZ, Yue M, Lynn JW, Liu LJ, Chen Y, et al. Temperature, magnetic field, and pressure dependence of the crystal and magnetic structures of the magnetocaloric compound $\text{MnFe}(\text{PGe})$. *Phys Rev B (Condensed Matter Mater Physics)* 2009;80(17):174415. doi:10.1103/PhysRevB.80.174415.
- [6] Planes A, Manosa L, Acet M. Magnetocaloric effect and its relation to shape-memory properties in ferromagnetic heusler alloys. *J Phys Condens Matter* 2009;21(23):233201 (29pp).
- [7] Rowe AM, Barclay JA. Ideal magnetocaloric effect for active magnetic regenerators. *J Appl Phys* 2003;93(3):1672–6. doi:10.1063/1.1536016.
- [8] Bouchekara H, Kedous-Lebouc A, Dupuis C, Allab F. Prediction and optimisation of geometrical properties of the refrigerant bed in an amr cycle. *Int J Refrig* 2008;31(7):1224–30. doi:10.1016/j.ijrefrig.2008.02.007.
- [9] Chernenko V, Pons J, Cesari E, Ishikawa K. Stress-temperature phase diagram of a ferromagnetic Ni–Mn–Ga shape memory alloy. *Acta Materialia* 2005;53(19):5071–7. doi:10.1016/j.actamat.2005.07.018.
- [10] Lyubina J, Schfer R, Martin N, Schultz L, Gutfleisch O. Novel Design of $\text{La}(\text{Fe}, \text{Si})_{13}$ alloys towards high magnetic refrigeration performance. *Adv Mater* 2010;22:3735–9. doi:10.1002/adma.201000177.
- [11] Chmielus M, Zhang XX, Witherspoon C, Dunand DC, Mullner P. Giant magnetic-field-induced strains in polycrystalline Ni–Mn–Ga foams. *Nat Mater* 2009;8:863–6. doi:10.1038/nmat2527.
- [12] Murray SJ, Marioni M, Allen SM, O'Handley RC, Lograsso TA. 6magnetic-field-induced strain by twin-boundary motion in ferromagnetic Ni–Mn–Ga. *Appl Phys Lett* 2000;77(6):886–8. doi:10.1063/1.1306635.
- [13] Sozinov A, Likhachev AA, Lanska N, Ullakko K. Giant magnetic-field-induced strain in NiMnGa seven-layered martensitic phase. *Appl Phys Lett* 2002;80(10):1746–8. doi:10.1063/1.1458075.
- [14] Khovaylo VV, Skokov KP, Koshkid'ko YS, Koledov VV, Shavrov VG, Buchelnikov VD, et al. Adiabatic temperature change at first-order magnetic phase transitions: NiMnGa as a case study. *Phys Rev B (Condens Matter Mater Phys)* 2008;78(6):060403. doi:10.1103/PhysRevB.78.060403.
- [15] Pasquale M, Sasso CP, Lewis LH, Giudici L, Lograsso T, Schlögl D. Magneto-structural transition and magnetocaloric effect in $\text{Ni}_{55}\text{Mn}_{20}\text{Ga}_{25}$ single crystals. *Phys Rev B* 2005;72(9):094435. doi:10.1103/PhysRevB.72.094435.
- [16] Vasil'ev AN, Bozhko AD, Khovailo VV, Dikshtein IE, Shavrov VG, Buchelnikov VD, et al. Structural and magnetic phase transitions in shape-memory alloys $\text{Ni}_{2+x}\text{Mn}_{20}\text{Ga}_{25}$. *Phys Rev B* 1999;59(2):1113–20. doi:10.1103/PhysRevB.59.1113.
- [17] Basso V, Sasso CP, Kupferling M. A peltier cells differential calorimeter with kinetic correction for the measurement of c_p (H, T) and Δs (H, T) of magnetocaloric materials. *Rev Sci Instr* 2010;81(11):113904. doi:10.1063/1.3499253.
- [18] Khovailo VV, Oikawa K, Abe T, Takagi T. Entropy change at the martensitic transformation in ferromagnetic shape memory alloys $\text{Ni}_{2+x}\text{Mn}_{1-x}\text{Ga}$. *J Appl Phys* 2003;93(10):8483–5. doi:10.1063/1.1556218.
- [19] Krenke T, Acet M, Wassermann EF, Moya X, Manosa L, Planes A. Martensitic transitions and the nature of ferromagnetism in the austenitic and martensitic states of Ni–Mn–Sn alloys. *Phys Rev B (Condens Matter Mater Phys)* 2005;72(1):014412. doi:10.1103/PhysRevB.72.014412.
- [20] Krenke T, Acet M, Wassermann EF, Moya X, Mañosa L, Planes A. Ferromagnetism in the austenitic and martensitic states of Ni–Mn–In alloys. *Phys Rev B* 2006;73(17):174413. doi:10.1103/PhysRevB.73.174413.
- [21] Sasso CP, Kuepferling M, Giudici L, Basso V, Pasquale M. Direct measurements of the entropy change and its history dependence in Ni–Mn–Ga alloys. In: *Proceedings of the 52nd annual conference on magnetism and magnetic materials*, Vol. 103. Tampa, Florida (USA): AIP; 2008. p. 07B306. doi:10.1063/1.2829011.
- [22] Dunand DC, Müllner P. Size effects on magnetic actuation in Ni–Mn–Ga shape-memory alloys. *Adv Mater* 2011;23(2):216–32. doi:10.1002/adma.201002753. URL, <http://dx.doi.org/10.1002/adma.201002753>.